1-1-1981

Correlation of pressure fluctuations at an impingement corner due to vortex-corner interaction.

Yuk-Pui Tang

CORRELATION OF PRESSURE FLUCTUATIONS AT AN IMPINGEMENT CORNER DUE TO VORTEX-CORNER INTERACTION

by

Yuk-Pui Tang

A Thesis
Presented to the Graduate Committee
of Lehigh University
in Candidacy for the Degree of
Master of Science
in
Mechanical Engineering

Lehigh University
August 1981

This thesis is accepted and approved in partial fulfillment of the requirements for the degree of Master of Science.

24 August, 1981
(date)

Professor in Charge

Chairman of Department

ACKNOWLEDGEMENTS

I am truly grateful to Dr. Donald Rockwell for his advice, encouragement and all the time he dedicated to my educational and personal growth.

The technicians, Mr. Jim Bunderla and Mr. Richard Towne, and the lab supervisor, Mr. Fred Wehden, were indispensible in constructing necessary pieces of apparatus and instrumentation. My sincere thanks goes to them for their efforts.

Thanks goes to all the members of the Mechanical Engineering and Mechanics Department, especially to Dr. Charles Knisely, who helped me in many ways. I am also indebted to Miss Sharon Cawley for her expert typing of this manuscript.

NOMENCLATURE

c_v	convective speed
f	frequency
$\tilde{F}$	fluctuating force
L	cavity length
$\tilde{M}$	fluctuating moment about ($x/\lambda = 1$, $y/\lambda = 1$)
$\tilde{P}$	fluctuating pressure
Re	Reynolds number
t	time
T	period of oscillation
$\tilde{u}$	fluctuating longitudinal velocity component
$\bar{u}$	mean longitudinal velocity component
U	free-stream velocity
x	streamwise coordinate (at corner)
x'	streamwise coordinate (at separation)
y	transverse coordinate (at corner)
y'	transverse coordinate (at separation)
z	spanwise coordinate (at corner)

Greek

β	fundamental frequency of shear layer oscillation
Γ	circulation
$\Delta\epsilon$	increment in ϵ
ϵ	transverse offset of corner
θ	momentum thickness

λ	wavelength
π	3.14159...
ρ	density of water
ϕ	phase angle

Subscripts

$( )_{\beta}$	at fundamental frequency of oscillation
$( )_{o}$	at separation ($x' = 0$)
$( )_{\tilde{p}}$	pertaining to pressure fluctuation
$( )_{rms}$	root mean square value
$( )_{R}$	at reference station ($x' = 18\ \theta_R$)
$( )_{\tilde{u}}$	pertaining to longitudinal velocity fluctuation

TABLE OF CONTENTS

LIST OF FIGURES

LIST OF FIGURES (Cont'd)

ABSTRACT

The impingement of concentrations of vorticity upon a corner is studied using simultaneous flow visualization and correlation of pressure fluctuations, revealing the relations between the instantaneous pressure fields along the top and front faces of the corner and the instantaneous distortion of the incident vortex.

By varying the transverse offset of the corner relative to the incident vortex, several distinct and consistent patterns of incident vortex-corner interaction are evident. The corresponding form and phasing of the instantaneous pressure fields are strongly dependent upon the nature of the vortex-corner interaction, though the maximum amplitude on the top and front faces is always of order $\rho \tilde{u}_{max} U$ of the approach flow. For certain interactions, there is separation of flow from the edge of the corner, as well as from the front face of the corner, leading to secondary-vortex formation and corresponding peaks in the local pressure fields.

By integrating the instantaneous pressure fields along the top and front faces of the corner, the phasing between the respective forces is shown to exhibit varying degrees of dipole-like behavior, depending upon the character of the incident vortex-corner interaction. Amplitudes of the corresponding moments of the pressure fields are remarkably insensitive to this interaction.

INTRODUCTION

The nature of large scale coherent structures in unstable laminar and turbulent shear layers has received considerable attention (see review of Roshko 1978), but the interaction between these vortical structures and various surfaces is not well understood; yet such interactions are central to characterizing the dynamic loading of the surface and the associated noise generation. Recent studies in this direction include vortex- (slender) leading edge interaction (Ziada and Rockwell 1981), as well as the nature of the unsteady shear layer upstream of a corner configuration (Knisely and Rockwell 1979, 1981). These investigations show that insertion of an edge or corner in the shear layer has a deterministic role in organizing the flow events in upstream regions of the shear layer. However, the relationship between distortion of vortices incident upon an edge or corner and the induced pressure fields along the corresponding surfaces has remained uninvestigated.

The purpose of this investigation is to visualize the distortion of vortices incident upon a corner for various transverse locations of the corner with respect to the incident vortex, as well as associated concentrations of (opposite) vorticity arising from the corner interaction; simultaneously, the instantaneous pressure fields are characterized, allowing detailed insight into the intimate relation between vortex interaction and induced pressure.

EXPERIMENTAL SYSTEM AND TECHNIQUES

Test Section and Flow Parameters

Figure 1 shows an overall view of the water channel test section. The acceleration ramp and the impingement corner were housed inside a 24 cm wide plexiglass insert to minimize the influence of channel wall boundary layers. The water level was maintained a height of 112 θ_R above the separation edge ($y' = 0$) where θ_R is the reference momentum thickness at the streamwise station 18 θ_R upstream of the impingement corner. Extensive velocity spectra were acquired in the freestream to ensure that there was no contamination from free surface effects (Knisely and Rockwell 1981). A laminar boundary layer was achieved at separation with free-stream velocity of 18.3 cm/sec. The corresponding Reynolds numbers were $Re_{\theta_o} = 141$ (at separation) and $Re_{\theta_R} = 257$ (at the reference station one wavelength upstream of impingement). Power spectra of free-stream velocity fluctuations revealed a total (integrated spectral) turbulence level of less than 0.1 percent, primarily concentrated at frequencies well below those of interest in this study.

A relatively short cavity length of $31\theta_R$ was selected for two reasons: the flow upstream of impingement could be maintained essentially two-dimensional; and "jitter", or irregularity, in the vortex impingement pattern that becomes pronounced at longer cavity lengths (Knisely and Rockwell 1981) could be precluded. A range of vortex-corner interaction patterns were studied in detail by selecting different vertical offsets of the impingement corner relative

to the separation edge. High, medium and low corner positions correspond to $\epsilon/\theta_R = 3.3$, 1.1 and -1.1, respectively, where ϵ is defined in Figure 1. The fundamental frequency of vortex formation remained the same, regardless of corner height.

Visualization Technique

Vortex impingement upon the corner was visualized using the dye injection technique. Food color dye was laid on the surface of the acceleration ramp to generate continuous streaklines. An Instar dual camera television system having vertical and horizontal sweep frequencies of 120 Hz and 25.2 Hz respectively, with split screen capability, recorded the corner region activity and the simultaneous pressure/velocity fluctuation traces were displayed on a storage oscilloscope. At a framing rate of 120 frames per second and a resolution of 250 lines, the recording had an uncertainty due to the finite time between frames of $\pm$ 1.2% of the period of vortex formation. All photos shown herein were obtained by taking 4" x 5" Polaroids of the image on the video screen at approximately the same scale unless otherwise stated.

Surface Pressure Measurement Devices

In the immediate region of the corner, large streamwise gradients of pressure can occur, depending on the nature of vortex distortion. Consequently, a design incorporating a rotating disc arrangement was constructed to measure pressure at a relatively large number of stations over a small area near the corner. The

model consists of two pressure "valves", one on the top, the other on the front face of the corner; only the top face arrangement is described here. The components are: an outer brass cover plate, a brass disc, and a thin rubber gasket as shown in Figure 2. The main element is the thin flanged-disc with thirteen 0.16 cm diameter holes drilled through its surface to serve as pressure taps; they are arranged in a pattern designed to achieve the desired "effective" spacing of pressure taps. That is, the angular spacing between adjacent holes is determined so that a sector covered by each hole does not overlap with that covered by the adjacent ones. Each of these thirteen holes is located at a different radial distance from the disc center with an increment of 0.16 cm to form a spiral pattern, covering a complete revolution. Placed underneath the disc is a thin rubber gasket with a 0.16 cm x 2.06 cm slot. A 5.72 cm square cover plate with a circular cutout is used to hold the disc and the gasket together against the plexiglass corner structure by means of four screws. A 0.16 cm diameter circular passage is drilled at the middle of the channel cut into the plexiglass corner to connect with the side mounted pressure transducer. Since only the disc is free to rotate, proper angular orientation of the disc allows only one of the thirteen taps to be sensed by the pressure transducer. Thus, a pressure tap can be positioned at any of thirteen discrete locations along a streamwise line by simply rotating the disc. Although not shown in Figure 2, the vertical surface of the corner is equipped with an

assembly identical to that described above, in order to provide simultaneous pressure measurement on both surfaces of the corner.

Each pressure valve system was tested in a water channel with zero flow to determine its natural frequency and damping ratio. A Kulite XCS-190-2D pressure transducer having its diaphragm coated with Paralene was selected because of its small size and high natural frequency of 100 kHz. Transient responses for both the top valve system (shown in Figure 2), as well as the front valve system (i.e. on the front face of the corner), subjected to an impulse input, were recorded simultaneously and the corresponding cross-spectrum computed digitally. Results showed that the natural frequency is about 22 Hz with a damping ratio of no more than 0.07 for all taps. This corresponds to amplitude and phase distortions of 2 percent and 1.2 degrees, respectively, at the highest frequency of interest in the present investigation. The length of the line from a given tap to the face of the pressure transducer varies, depending on the tap chosen, but negligible time delay was measured between the front and the top tap when the maximum difference in passage length was chosen.

Two other corner pieces were built with fixed pressure taps positioned on both the front and top faces at 0.16 cm and 0.32 cm from the edge of the corner. The pressure tap on the top face had a lateral offset (in the z direction) of 0.36 cm (approximately 14 percent of the wavelength of the incident vortex) in order to accommodate the hidden passages leading to the pressure transducers.

Each corner piece replaced the aforementioned rotating disk arrangements, allowing pressure measurement very near the edge. The velocity fluctuation near separation was used as a reference signal to relate the phasing of pressure signals obtained from the two different corner pieces and the rotating disk system. Transient response characteristics of these two corner pieces were found to be identical to that of the rotating disk system, due to the relatively small length to diameter ratios of all pressure lines.

For the present experiments, use of every other available tap (7 out of 13) in the aforementioned rotating arrangement provided adequate resolution; therefore, this tap sequence was used for pressure measurement on both the front and top faces of the corner. These seven equally spaced (at 0.32 cm interval) taps cover a 1.91 cm path starting at 0.63 cm and ending at 2.54 cm from the edge of the corner; for pressure measurements very close (0.16 and 0.32 cm) to the corner, special corner attachments with fixed pressure taps were employed.

Measurement Techniques

A three-part measuring procedure allowed determination of both amplitude and relative phase of each local pressure fluctuation. First, for pressure measurement on the front face of the corner, the leading tap on the top face was used to provide a reference signal, recorded simultaneously with each of the seven

pressure signals from the front face. Secondly, the reverse was carried out; the leading tap on the front face served as reference tap in order to obtain pressure measurement on the top face. Finally, pressure measurements were taken "diagonally", using taps on both surfaces having the same distance from the edge of the corner. Therefore, a total of 21 sets of effectively simultaneous pressure signals were acquired. As for measurement very close to the edge, using the two corner pieces having fixed pressure taps located distances of 0.16 cm and 0.32 cm from thee dge, a hot film probe positioned at a fixed location near shear layer separation ($x' = 0$ in Figure 1) provided a reference signal; such a phase reference is necessary in relating these measurements to those acquired with the rotating disk system.

All the pressure signals and their accompanying reference signals were digitized, recorded, then processed using a cross-spectrum program to determine their amplitude and relative phase. Each sample contained approximately 115 cycles of oscillation and the resultant, ensemble-averaged spectrum had a frequency resolution of 0.16 Hz. The deliberate redundancy of the above measuring procedure allowed cross-checking the amplitude and phase measurements.

Velocity measurements were taken by means of DISA hot film probes (55R14) using a DISA 55D01 anemometer in conjunction with a DISA 55M25 linearizer. Velocity and pressure signals were filtered with negligible phase shift at the fundamental frequency of fortex formation and amplified by Krohn-Hite Model 3700 bandpass

filters and class A variable gain amplifiers.

A MINC computer with 64K floppy disk memory allowed real time spectral analysis. Resultant velocity or pressure spectra were ensemble-averaged (over 5 independent spectra) for improved statistical validity and displayed on a CRT terminal. On the other hand, most pressure signals, along with a simultaneous reference signal (either velocity or pressure signal), were sampled, digitized and stored on cassettes using a digital oscilloscope (Nicolet 1090A, 4K memory) in conjunction with an interface (Nicolet 232C) and a data cassette recorder (Techtran 8410). The stored data were later transferred to magnetic tapes and processed on a CDC 6400 digital computer via a cross-spectrum technique to determine the amplitude and phase of the pressure signal with respect to the reference signal.

NATURE OF UNSTEADY SHEAR LAYER INCIDENT UPON CORNER

To characterize the unsteadiness incident upon the impingement corner, a reference station was chosen a distance of approximately one disturbance wavelength upstream of impingement corresponding to 18 θ_R, where $\theta_R = 1.8\ \theta_o$; moreover, at this location, the amplifying disturbance had reached its saturation value. Distortion of the fluctuating vorticity field due to the downstream corner is negligible at this reference station; in a related study, Rockwell and Knisely (1979) found, using LDA and hydrogen bubble techniques, that the convective velocity and

distortion of the incident vortex were influenced only very near the corner-less than one wavelength upstream of it. Normalizing parameters employed herein are the reference momentum thickness (θ_R) and the wavelength (λ) of the shear layer approaching the corner. Figure 3(a) shows the mean velocity profile at the reference station, compared with the hyperbolic tangent profile, $\frac{u}{U} = [1 + \tanh(y-y_{0.5})/2\theta_R]/2$ (Michalke 1965). In Figures 3(b) and 3(c) the distributions of longitudinal velocity fluctuation ($\tilde{u}_{rms}$) and its phase ($\phi_{\tilde{u}}$) are compared with respective theoretical profiles based on the linear inviscid theory of Michalke (1965) at the local Strouhal number ($f\theta_R/U = .022$). With these well-posed conditions of the approach shear layer, the unsteady pressure field at the corner can be scaled accordingly.

TIME-AVERAGED PRESSURE DISTRIBUTIONS

Amplitude

Shown in Figure 4(a) are time-averaged amplitude distributions of the pressure fluctuation ($\tilde{p}(x)$ and $\tilde{p}(y)$) on both faces as a function of transverse offset of the corner, extending approximately one wavelength downstream of the edge of the corner. These amplitude distributions are normalized with respect to the maximum value experienced in all three cases ($\tilde{p}_{max}$), estimated to be the order of 10^{-3} psi = 0.42 ($\rho U^2/2$). Along the top face of the corner, the pressure maximum does not occur at the leading edge; instead, it tends to occur at larger x/λ for decreasing ε/θ_R. That is, when

a larger fraction of the incident vortex passes above the edge, the pressure peak tends to become more gradual and move further downstream. (As will be shown, the pronounced peak occurring at small x/λ for large offset ($\epsilon/\theta_R = 3.3$) is associated with a leading-edge separation process.) On the other hand, along the front face, the peak occurs at or very near the leading edge, with the exception of the largest offset ($\epsilon/\theta_R = 3.3$), where the low center of the incident vortex produces a corresponding peak well below the edge; at this same offset, there is an amplitude minimum at $y/\lambda = 0.6$ due to flow separation from the front face, to be visualized subsequently. For the lower values of offset ($\epsilon/\theta_R = -1.1$, 1.1), the pressure amplitude drops to approximately its minimum value by $y/\lambda = 0.5$, meaning that the major share of the fluctuation energy is distributed over approximately half a wavelength along the front face of the corner. Remarkable is the fact that the peak pressure amplitude $\tilde{p}_{max}$ on the top and front faces is of the same order of magnitude for all cases, being of the order of $\rho\tilde{u}_{max}U$, where $\tilde{u}_{max}$ is the maximum amplitude of the velocity fluctuation immediately upstream of impingement ($\tilde{u}_{max}/U = 0.076$), and U is the freestream velocity.

Phase

Time-averaged phase distributions are shown in Figure 4(b). Along the top face, the phase continuously increases in the streamwise direction for lower values of offset ($\epsilon/\theta_R = -1.1$, 1.1),

indicating a downstream travelling wave associated with that share of the incident vorticity swept downstream of the edge. Reliable phase data could not be acquired at the largest offset ($\epsilon/\theta_R = 3.3$) for $x/\lambda \gtrsim 0.35$, due to small pressure amplitudes of the organized wave; the flat phase distribution for $x/\lambda \lesssim 0.35$ is associated with leading edge separation and severe distortion, to be discussed. In contrast, the phase distributions along the front face (at $\epsilon/\theta_R = -1.1, 1.1$) show a mild decrease in the adjustment region very near the edge, and nearly constant values further from the edge; that is, away from the edge, the fluctuations respond nearly instantaneously (i.e. in phase) at all locations to the unsteadiness arising from the vortex edge-interaction. For the largest offset ($\epsilon/\theta_R = 3.3$), the minimum in the phase distribution (see Figure 4(a)) occurs at the same location as the aforementioned pressure minumum, both being linked to the onset of flow separation there; downstream of this location, the phase increases, indicating a wave travelling down into the cavity; this interpretation is compatible with visualization of Figure 6(c).

To examine the effect of the impingement corner on the convective speed of the vortices incident upon the corner, the phase of fluctuating velocity $\phi_{\tilde{u}}(x)$ was taken along the edge of the shear layer ($u/U = 0.95$); resultant distributions are given in Figure 5. For the offsets where the vortex is swept virtually intact past the edge ($\epsilon/\theta_R = -1.1$) and split at the edge ($\epsilon/\theta_R = 1.1$), the slope of the velocity phase, and therefore the convective

speed ($c_v = f/d\phi/dx \simeq 0.42\ U$), are not significantly affected by the corner interaction; moreover, there is reasonable agreement with the pressure phase $\phi_{\tilde{p}}(x)$ along the top face as seen in Figures 5(a) and 5(b). However, as shown in Figure 5(c) for the case where the incident vortex is swept down into the cavity, there is a radical change in the slope of $\phi_{\tilde{u}}$ at the edge, eventually readjusting to an essentially constant slope. The marked difference between this slope of $\phi_{\tilde{u}}(x)$ the flat slope of $\phi_{\tilde{p}}(x)$ near the edge is associated with the separation there (see Figure 7).

INSTANTANEOUS PRESSURE FIELDS

Representations of the instantaneous fluctuating pressure in the vicinity of the corner, shown in Figures 6(a), 6(b) and 6(c), were constructed using corresponding time-averaged amplitude and phase information given in Figures 4(a) and 4(b). The variations of these instantaneous pressure distributions with time, over one cycle of oscillation, are represented in 1/8 cycle intervals, starting at the top of Figures 6(a), 6(b) and 6(c). As shown, each pressure schematic is a composite of pressure distributions on both faces of the corner, with the front face (y axis) pressure distribution angled to the left and the top face (x axis) distribution displayed horizontally to the right; together, these distributions form an isometric view of the corner. (Note the blank region extremely close to the corner of extent ~.06 λ,

where no pressure taps could be instrumented.) Time-averaged amplitude ($\tilde{p}_{rms}$) envelopes are drawn symmetrically with respect to zero mean pressure; time-dependent ($\tilde{p}(t)$) amplitudes are indicated by the shaded areas. For all cases shown in Figures 6(a), 6(b) and 6(c), the leading tap on the top face is set arbitrarily at 0^o phase.

Flow visualization via dye injection was recorded using the video system to allow correlating the instantaneous pressure fields with the visualized, incident vortex. Using the dual camera, split-screen capability of the video system, the original video recordings simultaneously displayed the visualized flow and pressure traces from the active pressure taps. Selected visualization photos are included in Figure 6, covering the cyclic event at intervals of 1/4 cycle. All these photos have the same scale and cover a total distance of $\sim\lambda$ along the top and front faces of the corner, corresponding to the domain of pressure measurement.

Vortex Above Corner

For the negative corner offset of $\epsilon/\theta_R = -1.1$, visualization photos of Figure 6(a) show that the incident vortices experience very minor distortion as they are swept downstream past the corner. A slight distortion of the incident vortex in the form of a kink in the lower part of the dye marker is evident as the vortex passes the edge. Careful frame by frame study of the video recordings

suggests that the vortices actually climb up over the corner, whereby the center of a typical vortex is gradually displaced approximately 1.5 θ_R upward; this occurs over a streamwise distance of ~0.3λ upstream and downstream of the edge of the corner, and is due to the image vortex within the corner (Conlisk and Rockwell 1981). Such climbing is evident in the t=0 photo of Figure 6(a). Downstream of the edge, elongation of vortices in the streamwise direction is evident, enhanced by viscous effects at the wall; such elongation does not arise in purely inviscid simulations of vortex-surface interaction (Rogler 1978). In Figure 6(a) the wave-like nature of the instantaneous pressure distributions along the top face of the corner clearly depict the downstream convection of vortices. The initial rise of pressure amplitude immediately downstream of the edge is believed to be associated with the aforementioned "climbing" of the vortices near the edge as well as distortion of the unsteady field in that region. Subsequent decrease and leveling off of pressure amplitude further downstream is associated with increased distortion of the vortices as they interact with the viscous wall layer. In contrast to the top face of the corner, there is exponential drop of pressure amplitude along the front face; moreover, pressure fluctuations away from the edge ($y/\lambda \gtrsim 0.5$) are seen to respond instantaneously at all locations.

Vortex At Corner

Figure 6(b) illustrates the case of a small positive offset $\epsilon/\theta_R = 1.1$. Visualization shows that the center of the incident vortex is at essentially the same height as the edge. Substantial vortex distortion and apparent severing at the edge is evident. The lower portion of the vortex is swept downwards along the front face of the corner; flow separation from the front face is quickly induced, producing a concentration of vorticity of opposite sign. Together, these concentrations of vorticity form a counter-rotating vortex pair. There is little subsequent development of each vortex pair; moreover, these counter-rotating vortex pairs appear to "stack up" due to their very low convective speed, consistent with the small phase variation along the front face. Finally, vortex breakdown into turbulence was observed deep inside the cavity. From the instantaneous pressure distributions shown in Figure 6(b), it is apparent that except for the leading region of the front face (which is directly exposed to vortex impingement), the front face experiences nearly constant phase of pressure fluctuations. With regard to the top face of the corner, the portion of the clipped vortex that is downstream gives rise to a wave-like variation of pressure. Although it undergoes substantial distortion, visualization showed that this entity of rotational fluid remained distinguishable within several disturbance wavelengths downstream of the corner. Comparison of the $\tilde{p}(t)$ vs. x/λ variations of Figure 6(b) with those of Figure 6(a) reveals that

the form of the amplitude distributions as well as the phasing of the top face pressure fields are similar, the absolute amplitude being smaller for the case above because only a portion of the incident concentration of vorticity is swept downstream (i.e. Figure 6(b)).

Vortex Below Corner

At the largest positive offset $\epsilon/\theta_R = 3.3$, the vortex-corner interaction takes place primarily along the front face of the corner, as shown in Figure 6(c). The approaching vortex is severely distorted against the front face of the corner, then is swept downward into the cavity along the front surface. This distortion of the vortex gives rise to the first large peak of the pressure amplitude, having an extent approximately corresponding to the apparent diameter of the incident vortex. Subsequent downward motion of the distorted vortex results in an eruption of a counter-rotating secondary vortex from the wall region. In the corresponding pressure composites, it is evident that the secondary peak in the pressure distribution (at $y/\lambda \gtrsim 0.75$) along the front face is associated with this secondary vortex activity. Along the top face of the corner, the pressure amplitude rises and drops off sharply. Since the signal to noise ratio of the pressure fluctuations was relatively small (except very near the edge), amplitude and phase distributions in the region $x \gtrsim 0.35\lambda$ were not considered to be sufficiently accurate to be shown here.

However, near the edge, the pressure fluctuation is well-defined. In fact, examination of the instantaneous pressure fields of Figure 6(c) shows that the maximum pressure amplitudes on the top and front faces of the corner are π out of phase throughout the oscillation cycle, suggesting a well-defined dipole behavior.

In order to better understand the mechanism of flow around the edge, dye was introduced into the cavity from an existing pressure tap (0.16 cm from the edge) on the front face. Figure 7 shows the close-up visualization, along with the corresponding overall vortex impingement patterns. Four photos were taken at equal time intervals to cover approximately one-half an oscillation cycle, along with the corresponding overall vortex impingement patterns. The dye from the front pressure tap is seen to move upwards towards the edge, then separate to form a small vortex travelling downstream over the top face of the corner. The vorticity associated with this vortex has the same sense and a scale about one-tenth that of the large scale incident vortices. Associated with this leading edge separation process is a relatively large pressure peak on the top face as shown in Figure 6(c).

Effects of Larger Streamwise Length Scale (L)

Since the maturity, or degree of vorticity concentration, and therefore circulation Γ, of the incident vortex is a function of the impingement length scale L, its effective offset relative to the impingement corner (ϵ/θ_R) can be expected to change with

length L due to its image within the corner (Ziada and Rockwell 1981; Rogler 1974). Shown in Figure 8 is a visualized sequence covering nearly two cyclic events of vortex impingement at a geometrical offset of $\epsilon/\theta_R = 1.1$ for a longer cavity length ($L = 40\ \theta_R$). As shown, the impingement pattern is characterized by more mature roll-up of the incident vortex. The first incident vortex (see t=0 photo) is clipped slightly below its center to form a strong counter-rotating vortex pair along the front face; however, the second incident vortex (see t=T photo) approaches the corner at a slightly higher position, and no such counter-rotating vortex pair evolves. In general, it was found that at such longer cavity lengths, the vortex interactions at impingement exhibited the sort of variation shown in Figure 8. In such cases, the time-averaged measuring techniques employed in this study do not accurately represent the corresponding flow events, characterized by several frequent components (Knisely and Rockwell 1981); consequently, instantaneous pressure fields were not pursued for longer cavity length scales than those employed for studies described in Figures 3 through 7.

UNSTEADY FORCES AND MOMENTS ON THE CORNER

Unsteady forces on the corner can be examined by integrating instantaneous pressure distributions of Figures 6(a), (b), (c) on each surface of the corner. To illustrate the effects of the extent of the integration domain on the resultant force,

integrations were carried out over the leading 25%, 50%, 75%, and a full 100% of the pressure measurement domain, corresponding, respectively, to 1/4, 1/2, 3/4, and 1 wavelengths λ of the incident disturbance. Resultant forces, normalized with respect to the maximum value of all three corner offsets ($\epsilon/\theta_R = -1.1$, 1.1 and 3.3) are given in Figures 9(a), 9(b) and 9(c). As a larger share of the incident vortex is severed and swept down into the cavity (see Figures 6(a) through 6(c)), there is increased tendency for the instantaneous forces on the top and front surfaces of the corner to be π out of phase. In fact, for the case where nearly all of the incident vortex is swept downwards ($\epsilon/\theta_R = 3.3$), the maximum deviation from this π phase condition is only 0.12 π (see Figure 6(c)), regardless of the size of the domain over which the pressure is integrated. The physical reason for this remarkably consistent π phase difference can be seen be examining the instantaneous pressure distributions of Figure 7(c). On the top and front faces, the dominant fluctuation amplitudes occur very near the edge, and are π out of phase; moreover, the amplitude of the secondary peak on the front face (at $y/\lambda = 0.8$) is relatively small and tends to be in phase with the dominant peak on that face (at $z/\lambda = 0.25$). As for the cases where the incident vortex is severed at ($\epsilon/\theta_R = 1.1$), or passes over ($\epsilon/\theta_R = -1.1$), the edge, there is deviation from this π phase difference, though the general tendency for the forces on the front and top faces to be out of phase is evident.

Integrated elemental moments acting on the corner, associated with the instantaneous pressure distributions on the corner, are determined by taking elemental moments about the point of intersection (inside the corner) of two perpendicular lines drawn through $x/\lambda = 1$ and $y/\lambda = 1$ (see Figure 7 for terminology). Fluctuating moments about this particular point emphasize the role of near edge events. Results are presented in a similar manner as the force fluctuations, using four different-sized domains. Results of fluctuating moments for corner offsets $\epsilon/\theta_R = -1.1$, 1.1 and 3.3 are shown in Figures 10(a), 10(b), and 10(c), respectively. In general, the fluctuating moments are found to have very similar magnitude and are not strongly influenced by the size of domain for all three corner offsets.

FEEDBACK NEAR SEPARATION

It is well known that the presence of the downstream impingement corner, along with the separation edge upstream, form a closed-loop feedback system promoting self-sustained oscillation of the shear layer. As shown in the series of Figure 7, vortex impingement causes redistribution of vorticity; consequently, velocity perturbations can be sensed in the sensitive region near separation. These velocity perturbation, in turn, modulate the development of the shear layer.

To investigate the effect of the transverse corner offset on the strength of the induced velocity, a hot film probe was positioned at separation to detect the velocity fluctuation when

the corner offset ϵ/θ_R was set at -1.1, 0, 1.1, 2.2 and 3.3. As shown in Figure 11, total root mean square of the velocity fluctuation increases asymptotically from 0.3% of U_∞ to 0.7% of U_∞ with increasing positive corner offset. Apparently, the strength of the feedback is proportional to the degree of vortex distortion at impingement. It should also be noted that large positive offset results in the appearance of detectable half harmonics of the fundamental frequency of oscillation β as depicted in Figure 11. With the vortex impacting on a rigid surface such as the case for $\epsilon/\theta_R = 3.3$ shown in Figure 6(c), the vortex distortion as well as the upstream velocity feedback is maximized.

SUMMARY OF VORTEX-CORNER INTERACTION MECHANISMS

The range of vortex-corner interactions described and shown in Figures 4 through 8 suggest the following concepts:

a. As the core of a vortex impinges upon and is swept past a corner, it induces pronounced negative pressure, both on front and top faces near the edge of the corner. This is dramatically depicted for the front face in: Figure 6(a) (t = 1/4T); Figure 6(b) (t = 1/4T); and Figure 6(c) (t = 0). For the top face, it is shown in: Figure 6(a) (t = 1/2T, 7/8T) and Figure 6(b) (t = 1/2T, 3/4T). In the event that the incident vortex impinges below the corner, there is also pronounced negative pressure on the front face, shown in Figure 6(c) (t = 0); moreover,

the eventual eruption of the boundary layer produces a counter-rotating vortex that induces a negative pressure at the (y/λ) location of its center, depicted in Figure 6(c) ($t = 7/8T$).

These observations agree with intuitive and conceptual models of convecting vortices, for which no direct visual vortex-pressure phase correlations have been available for confirmation (Lau et al. 1972; Lush 1973; Fuchs 1973). There are simulations of the phasing of of pressure fluctuations induced by convection of single, discrete vortex in a free jet (Lush 1973; Fuchs 1973) and past a corner (Conlisk and Rockwell 1981). In the case of the free jet, a negative pressure perturbation is induced in the core and entrainment region as the center of the vortex passes by (Lau et al. 1972); for the discrete vortex-corner interaction, such phasing cannot be accurately predicted, because the nature and deformation of the distributed vorticity of the incident vortex is dominant (Conlisk and Rockwell 1981). However, for the vortex travelling intact along the top face of the corner, the minor deformation of the vortex allows simulation of the phasing of induced negative pressure using a discrete vortex and its image, as, for example, carried out by Lush (1973). Though the amplitude predicted by his model requires

modification to account for mean velocity effects (Fuchs 1973), the phase of the pressure relative to location of center of the vortex is properly predicted, in agreement with the intuitive model of Lau et al. (1972), and the experimental observations herein: i.e. the center of the vortex corresponds to maximum negative pressure (e.g. see Figure 6(a)).

b. The order of magnitude of the maximum pressure fluctuation $\tilde{p}_{max}$ induced near the edge of the corner on both the top and front faces is the same, and is $\tilde{p}_{max} \simeq 2.8\rho\tilde{u}_{max}U$, where $\tilde{u}_{max}$ is the maximum amplitude of the velocity fluctuation in the shear layer just upstream of impingement and U is free-stream velocity.

c. In cases where significant fraction of the incident vortex concentration is swept downstream along the top face of the corner (e.g., Figures 6(a) and 6(b)):

   (i) The amplitude of the corresponding pressure fluctuations along the top face is smaller for smaller fractions of the concentrated vorticity swept downstream (Figure 6(b) relative to Figure 6(a)). This trend is associated not only with smaller strength (circulation), but also increased distortion,of the vorticity concentration swept downstream (compare Figure 6(b) with Figure 6(a)).

This increased distortion is associated with a decrease in slope of phase variation (decrease in $d\tilde{\phi}_p/dx$), corresponding to an increase in phase speed of the vorticity concentration (compare Figures 6(a) and 6(b)).

(ii) Along the front face of the corner, the amplitude of the pressure drops off much more rapidly than along the top face, decaying to about one-fourth its maximum value at a distance of one-half wavelength from the edge of the corner (see Figures 6(a) and 6(b)); this rate of drop-off is several times that occurring along the top face. Away from the edge of the corner, pressure fluctuations tend to be in phase at all spatial locations along the front face.

d. In the event that nearly all of the incident vorticity is swept below the corner (see Figure 6(c)), the following are evident:

(i) Maximum pressure occurs at the location of the center of the vortex (see Figure 6(c), $t = 0$); moreover; eventual eruption of the boundary layer from the front face results in formation of a counter-rotating vortex pair and a secondary maximum of fluctuating pressure (see Figure 6(c), $t = 7/8T$).

(ii) This counter-rotating vortex pair travels downwards along the front face ($y/\lambda \gtrsim 0.7$) with a phase speed $c_v/U = 0.25$.

(iii) Very near the edge of the top face of the corner, large amplitude pressure fluctuations are induced, being associated with flow separation from the edge; downstream of this region, the pressure amplitudes are extremely small.

e. With regard to the forces (integrated fluctuating pressures) exerted upon the top and front faces of the corner, they tend to be π out of phase; for the case where the major share of the incident vortex is swept below the corner, the π phase condition is satisfied with maximum deviation being $\sim 0.1\pi$, regardless of the size of the integration domain (see Figures 9(a), (b), (c)).

f. As for the fluctuating moments acting upon the corner, taken about a location to emphasize unsteady events in the vicinity of the edge, the amplitudes of the moments are remarkably insensitive to the nature of the vortex-edge interaction (i.e. fraction of incident vorticity swept above and below the corner) (see Figure 10). However, the phase difference between the moments is significant, with consistently increasing phase advance for increasing fraction of incident vorticity swept below the corner.

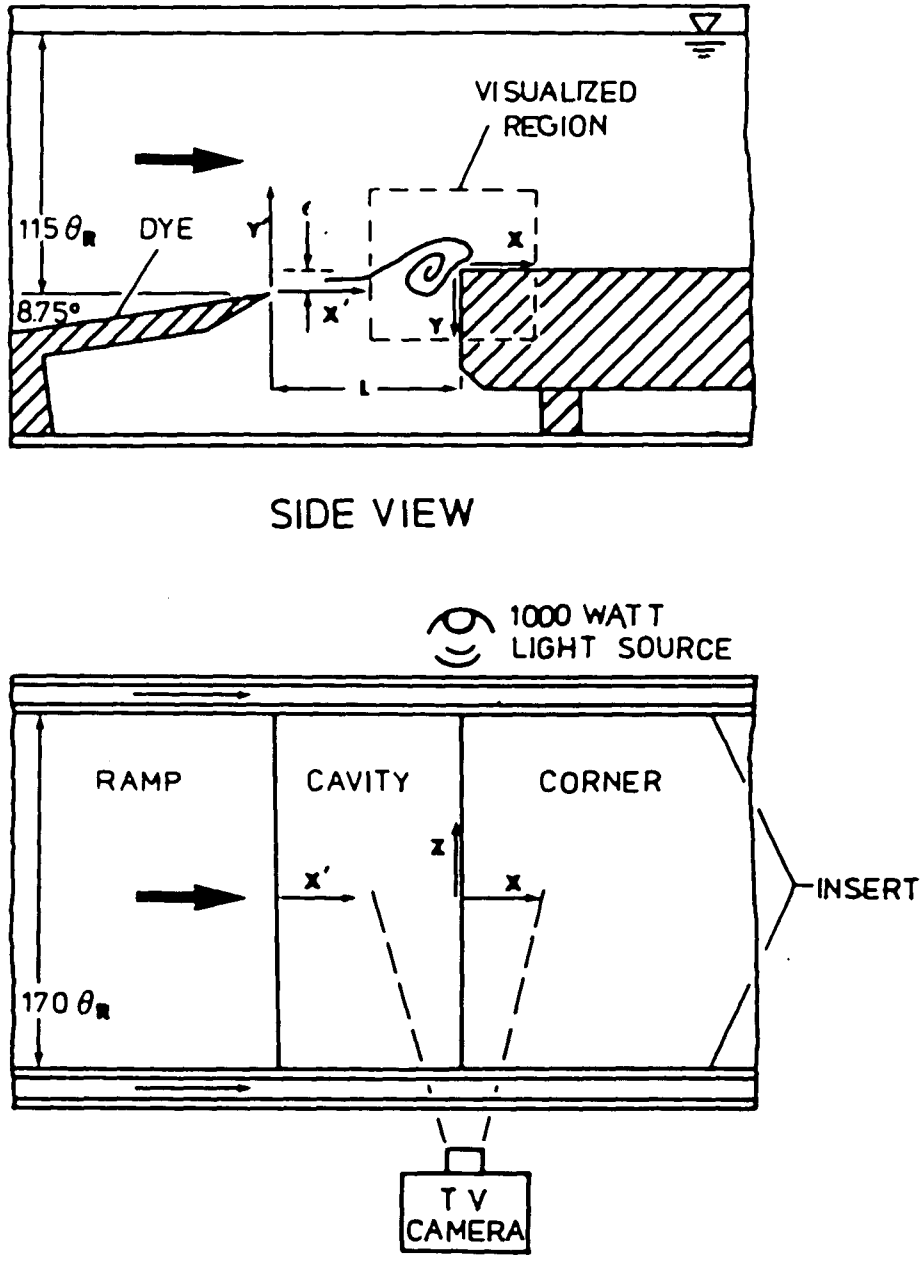

Figure 1: Overall view of the experimental test section and lighting arrangement for visualization.

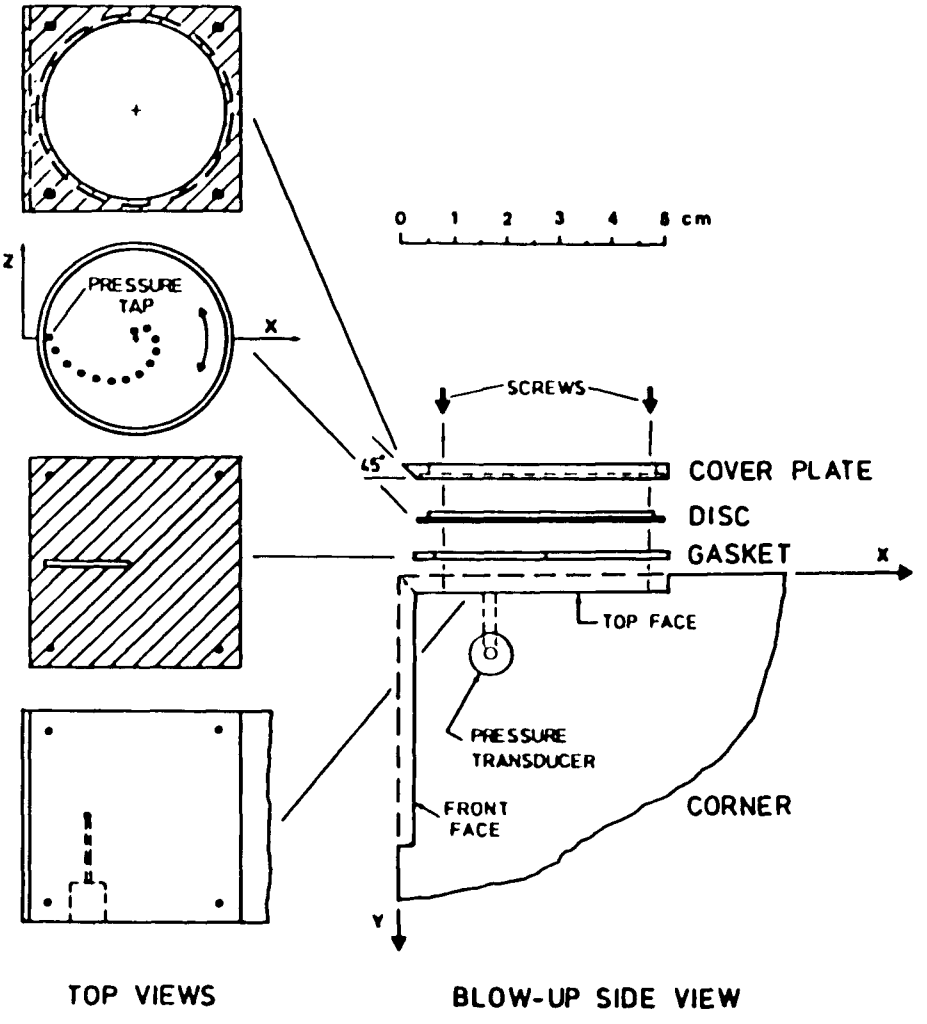

Figure 2: Rotating disk arrangement for measurement of distributions of fluctuating pressure over small domains near the edge of the corner.

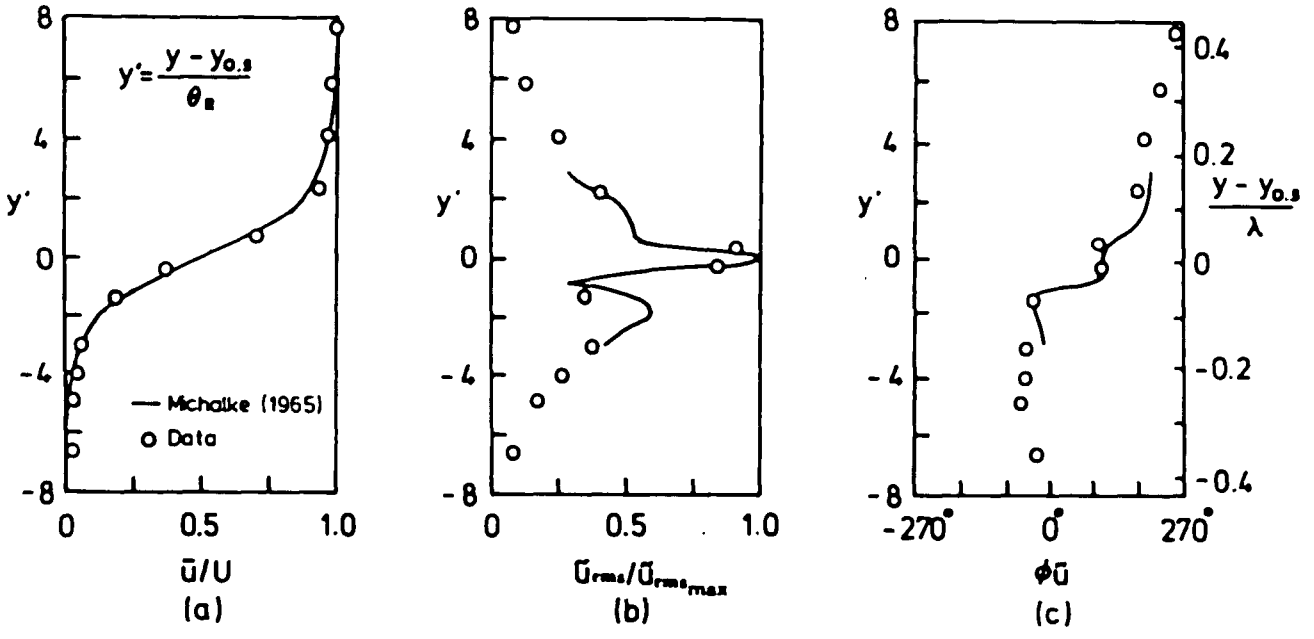

Figure 3: Profiles of mean and fluctuation parameters of the approach shear layer: (a) normalized mean velocity profile; (b) normalized distribution of longitudinal velocity fluctuation; and (c) phase distribution of the longitudinal velocity fluctuation. All distributions taken at reference station $x'/\theta_R = 13$. $\epsilon/\theta_R = 1.1$; $L/\theta_R = 31$.

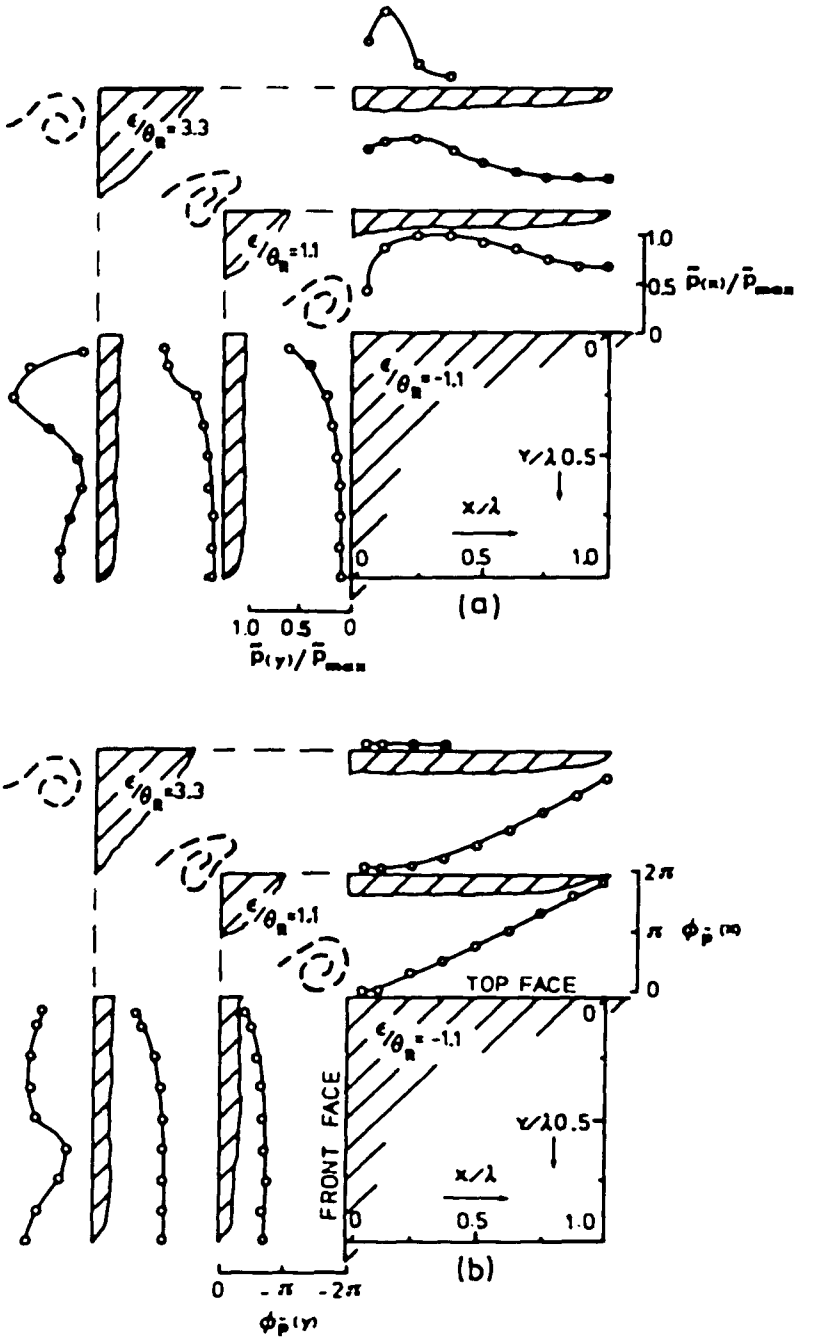

Figure 4: Distributions of: (a) time-averaged amplitudes; and (b) time-averaged phase of pressure. Both distributions shown along the top (x) and front (y) faces of the impingement corner for $\epsilon/\theta_R = -1.1$, 1.1 and 3.3 at $L/\theta_R = 31$.

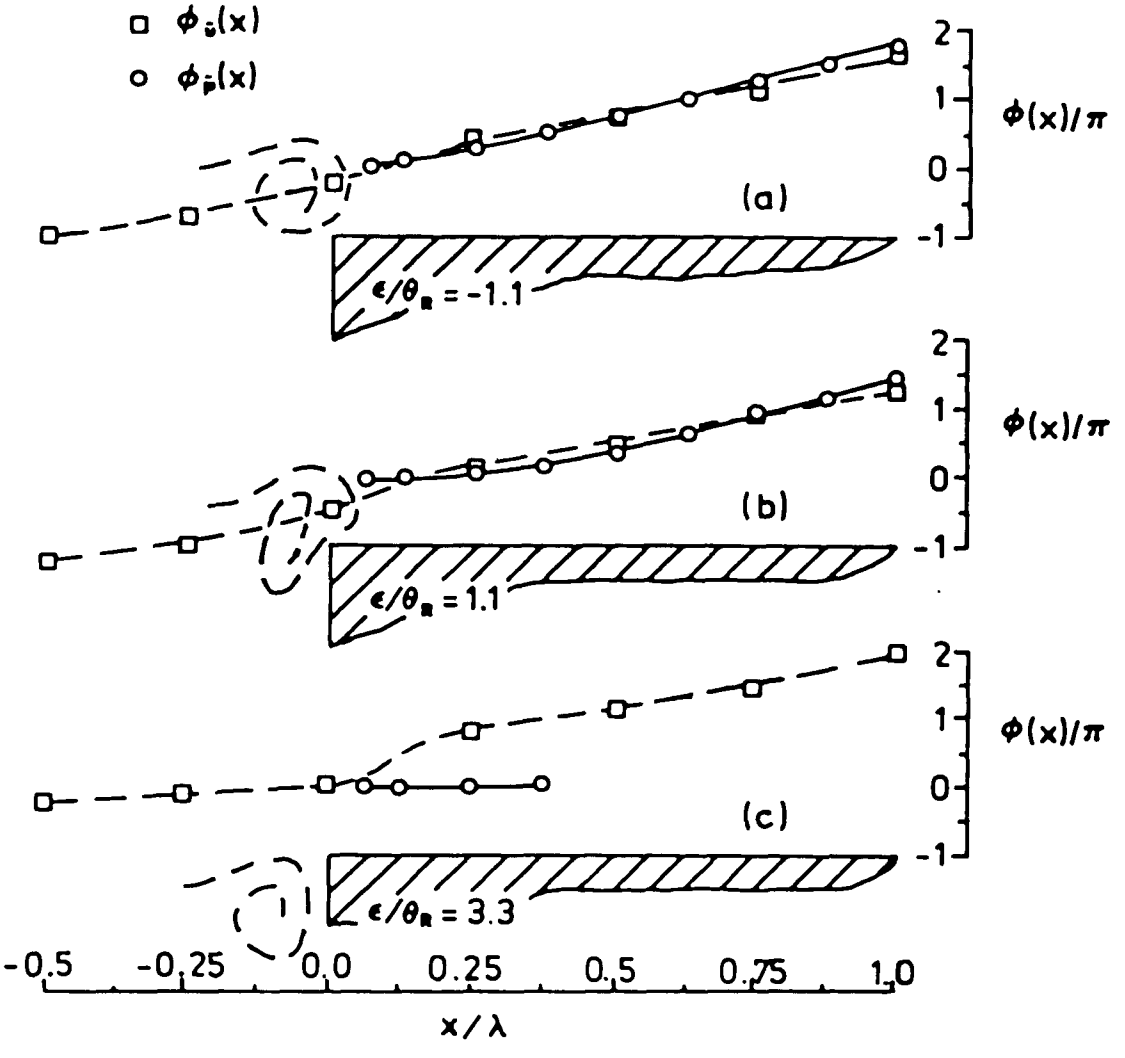

Figure 5: Streamwise phase distributions of: fluctuating velocity $\phi_{\tilde{u}}(x)$ taken along edge of shear layer; and fluctuating pressure $\phi_{\tilde{p}}(x)$ taken along wall. $\epsilon/\theta_R = -1.1$, 1.1 and 3.3. $L/\theta_R = 31$.

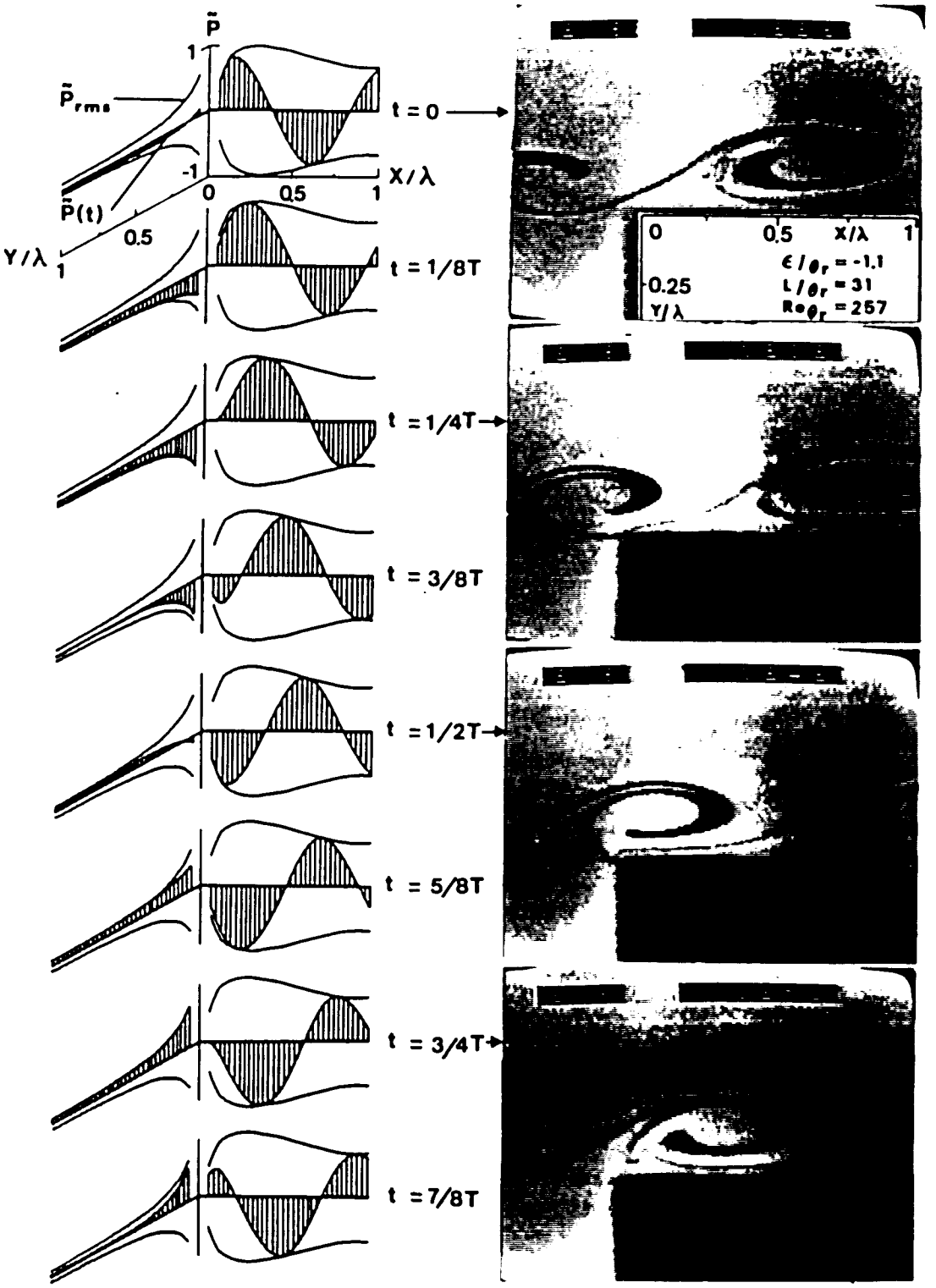
$\tilde{P}$
1
$\tilde{P}_{rms}$
-1
0
0.5
1
X/λ
$\tilde{P}(t)$
0.5
Y/λ
1
t = 0
t = 1/8T
t = 1/4T
t = 3/8T
t = 1/2T
t = 5/8T
t = 3/4T
t = 7/8T
0
0.5
X/λ
1
0.25
Y/λ
$\epsilon/\theta_r = -1.1$
$L/\theta_r = 31$
$Re_{\theta_r} = 257$

FIG. 6 (a)

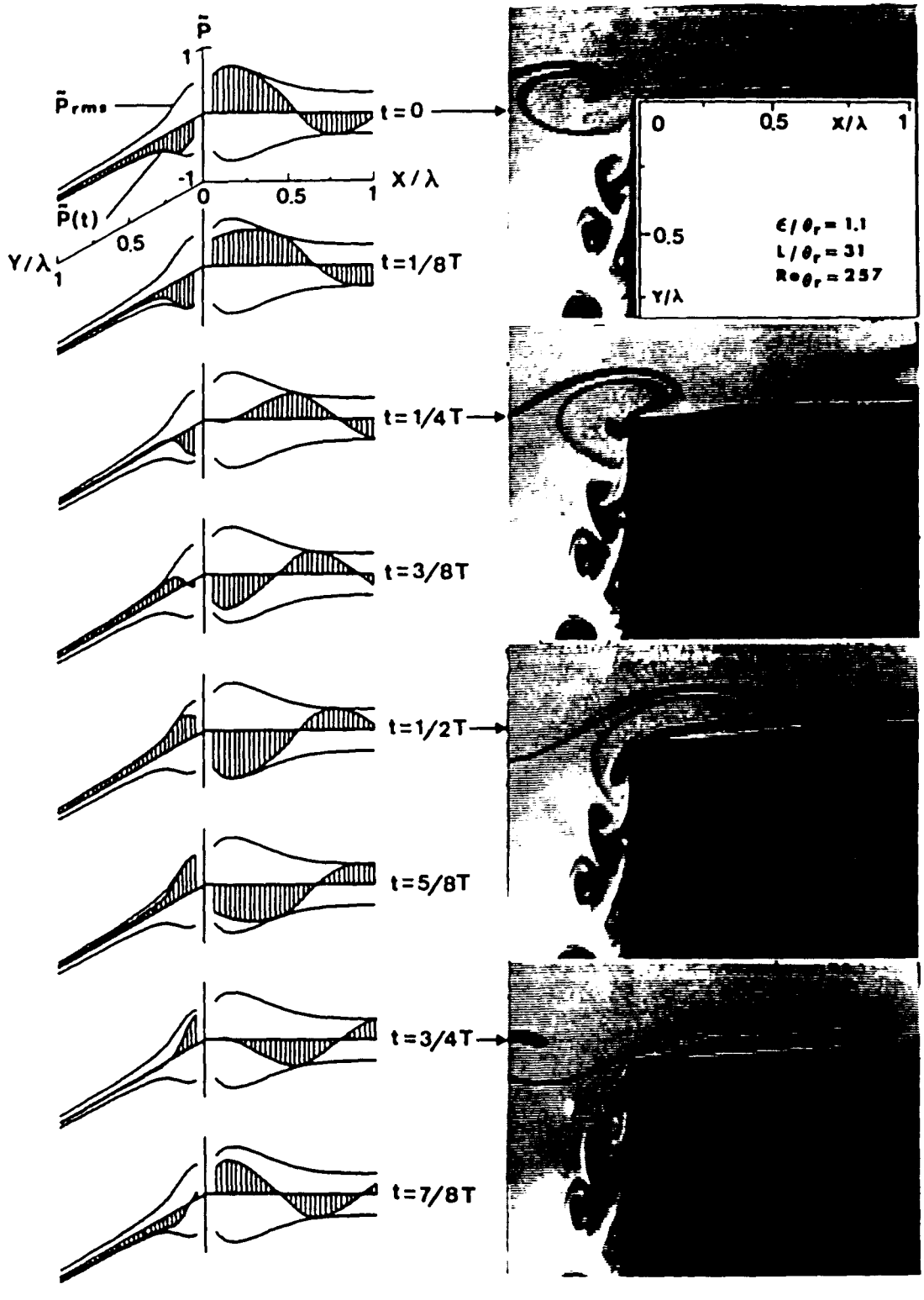
$\tilde{P}$
1
$\tilde{P}_{rms}$
t = 0
-1
0
0.5
1
X / λ
$\tilde{P}(t)$
Y/λ
0.5
1
t=1/8T
t=1/4T
t=3/8T
t=1/2T
t=5/8T
t=3/4T
t=7/8T
0
0.5
X/λ
1
0.5
Y/λ
$\epsilon/\theta_r = 1.1$
$L/\theta_r = 31$
$Re_{\theta_r} = 257$

FIG. 6 (b)

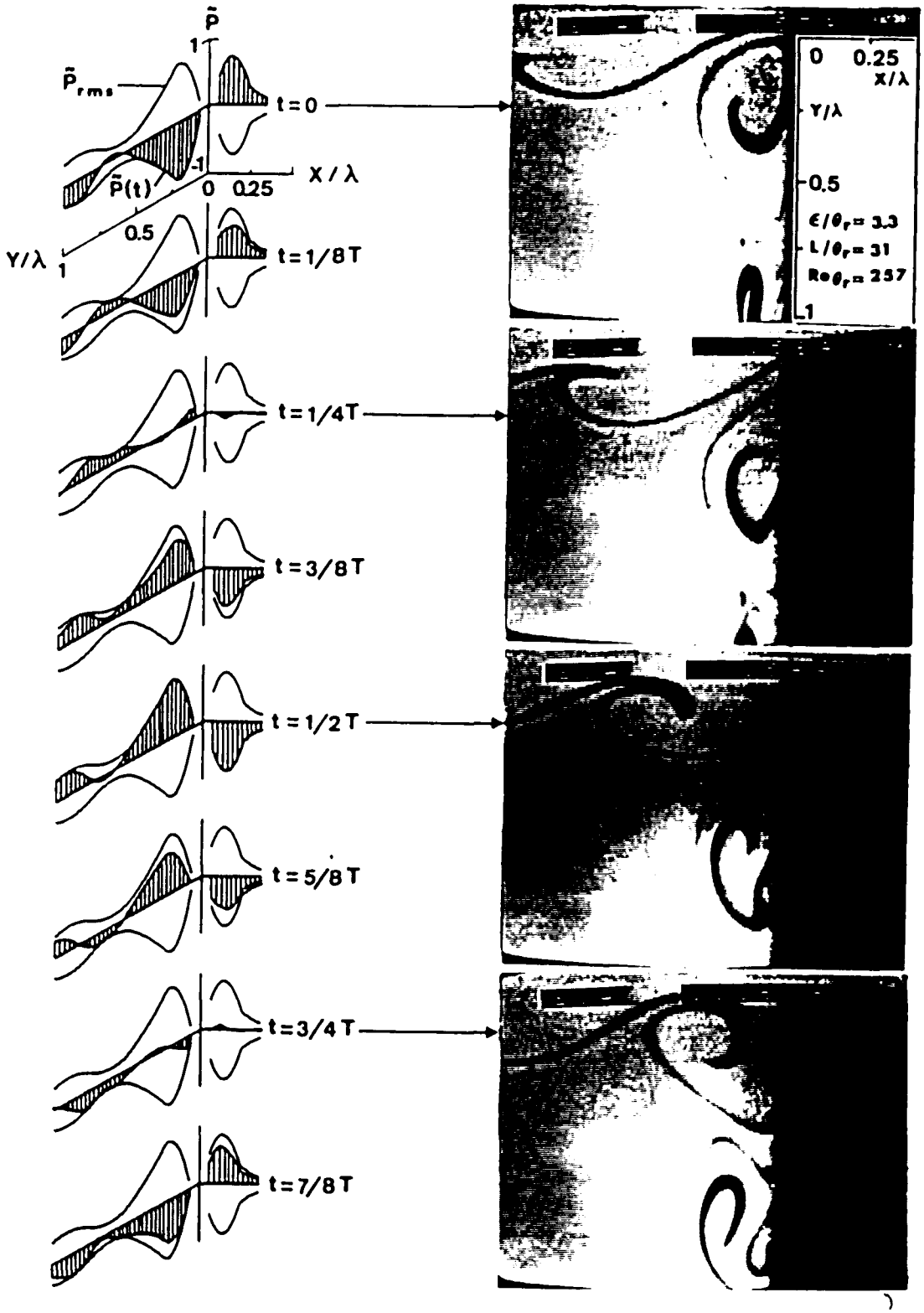
$\tilde{P}$
1
$\tilde{P}_{rms}$
t = 0
-1
$\tilde{P}(t)$
0 0.25
X / λ
Y/λ
0.5
1
t = 1/8 T
t = 1/4 T
t = 3/8 T
t = 1/2 T
t = 5/8 T
t = 3/4 T
t = 7/8 T
0 0.25
X/λ
Y/λ
0.5
1

FIG. 6 (c)

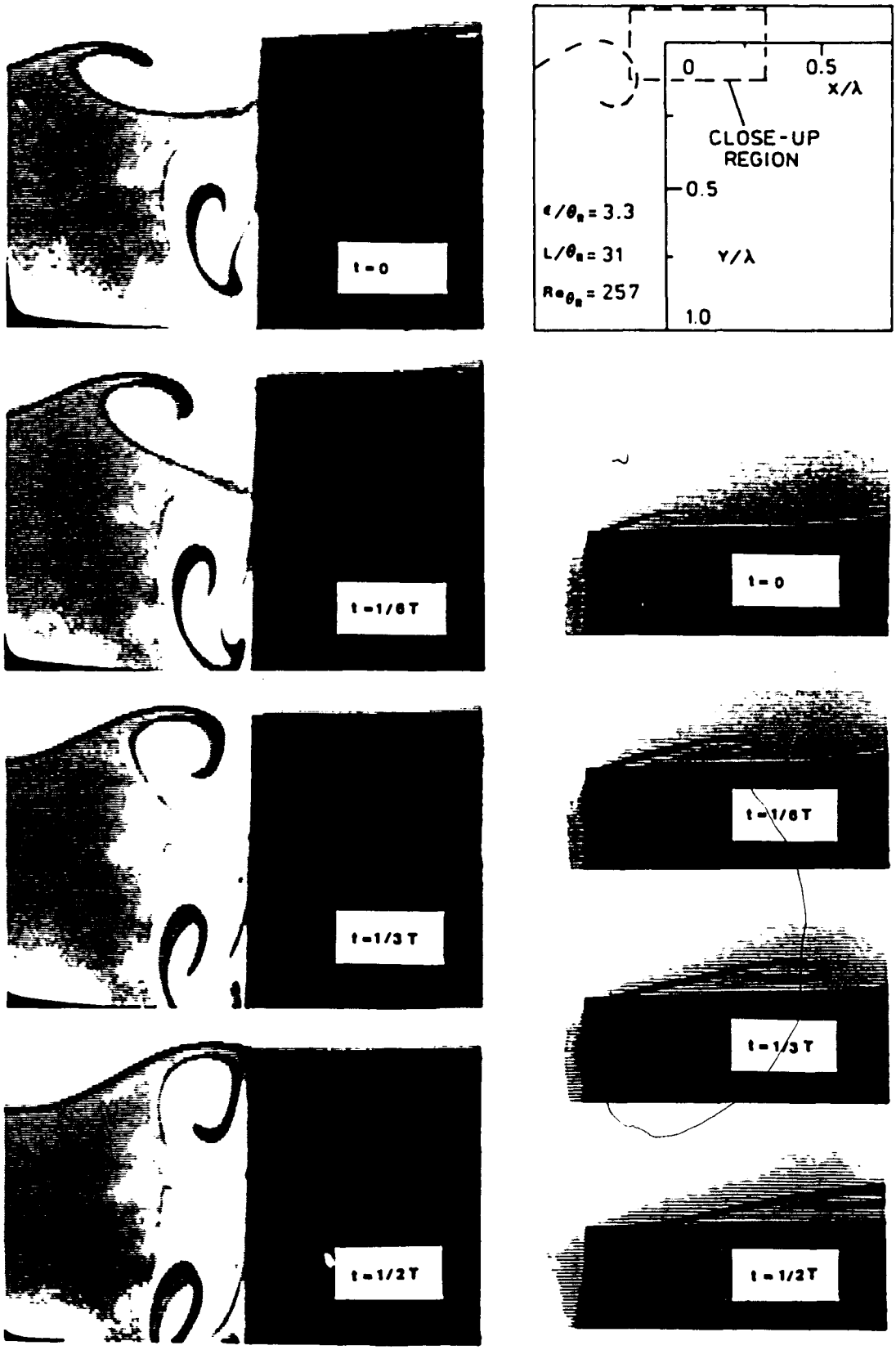
t = 0
t = 1/6 T
t = 1/3 T
t = 1/2 T
0
0.5
X/λ
CLOSE-UP
REGION
0.5
Y/λ
1.0
$\epsilon/\theta_s = 3.3$
$L/\theta_s = 31$
$Re_{\theta_s} = 257$
t = 0
t = 1/6 T
t = 1/3 T
t = 1/2 T

FIG. 7

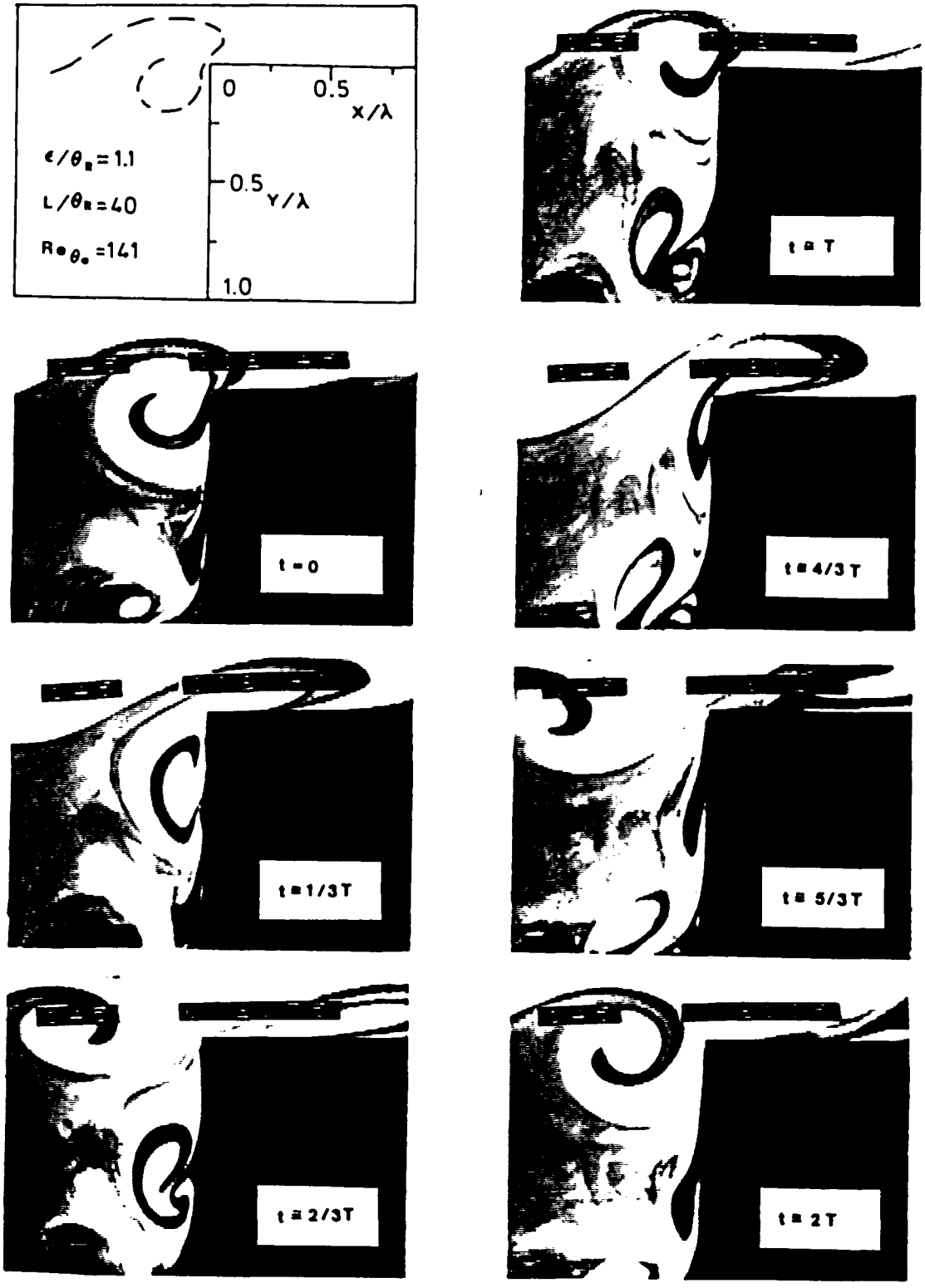
0
0.5
x/λ
$\epsilon/\theta_B = 1.1$
$L/\theta_B = 40$
$R\theta_0 = 141$
0.5
y/λ
1.0
t = T
t = 0
t = 4/3T
t = 1/3T
t = 5/3T
t = 2/3T
t = 2T

FIG. 8

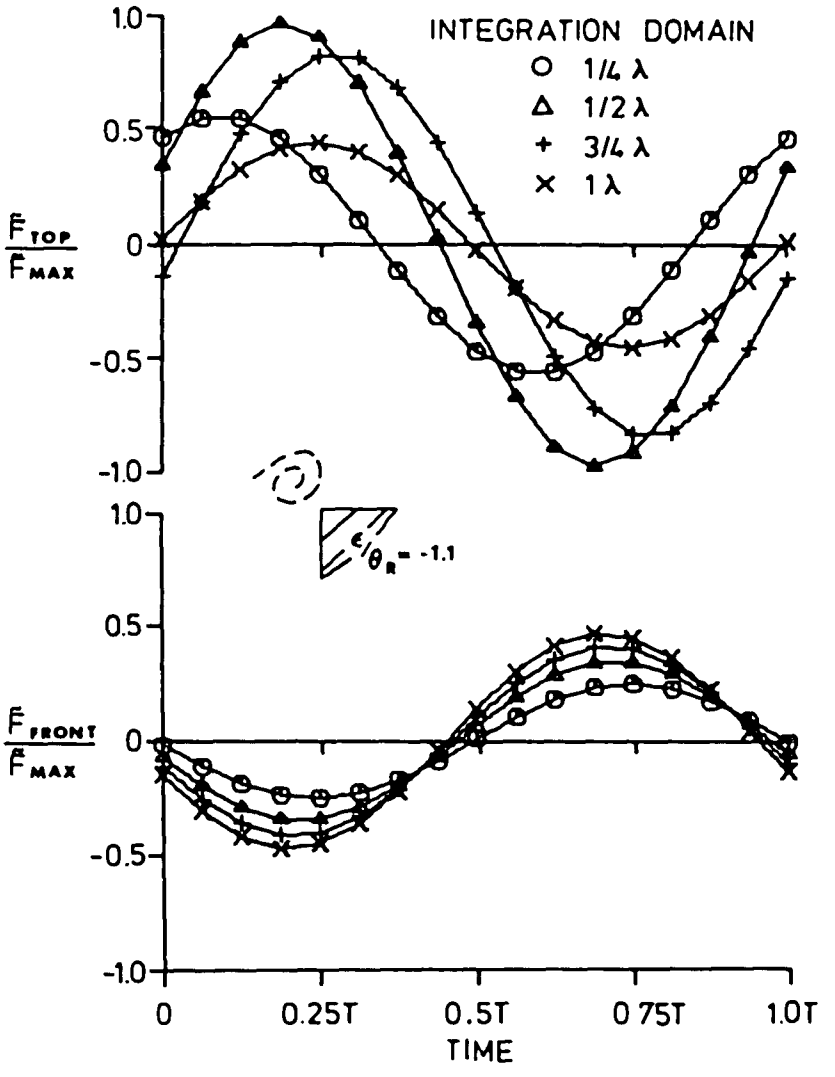

Figure 9a: Periodic forces ($\tilde{F}$) on top and front faces of the corner as a function of size of integration domain. $\varepsilon/\theta_R = -1.1$, $L/\theta_R = 31$.

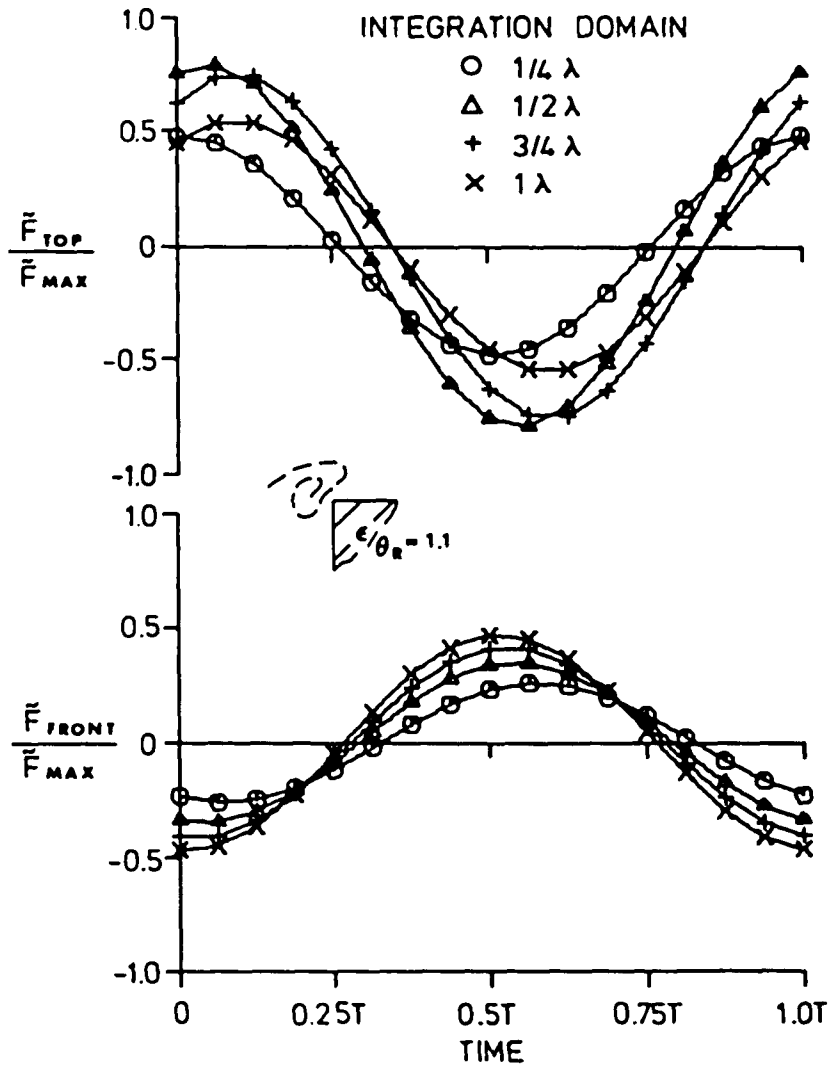

Figure 9b: Periodic forces ($\tilde{F}$) on top and front faces of the corner as a function of size of integration domain. $\epsilon/\theta_R = 1.1$, $L/\theta_R = 31$.

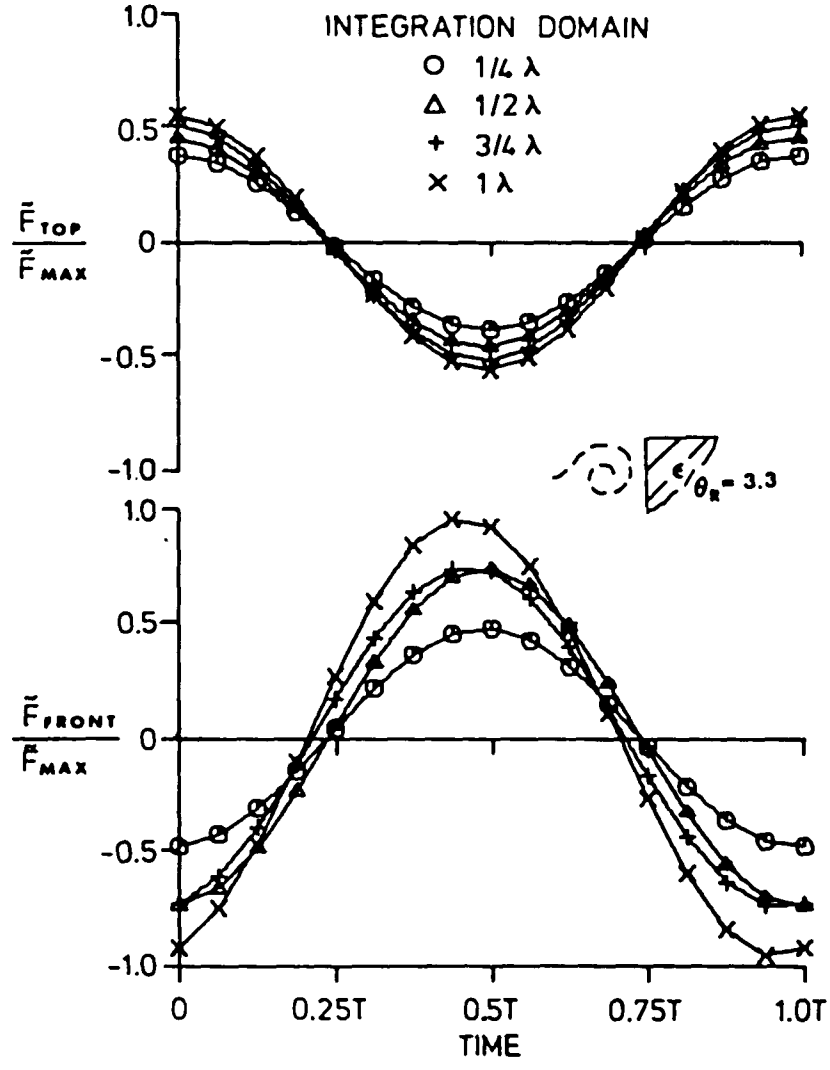

Figure 9c: Periodic forces ($\tilde{F}$) on top and front faces of the corner as a function of size of integration domain. $\epsilon/\theta_R = 3.3$, $L/\theta_R = 31$.

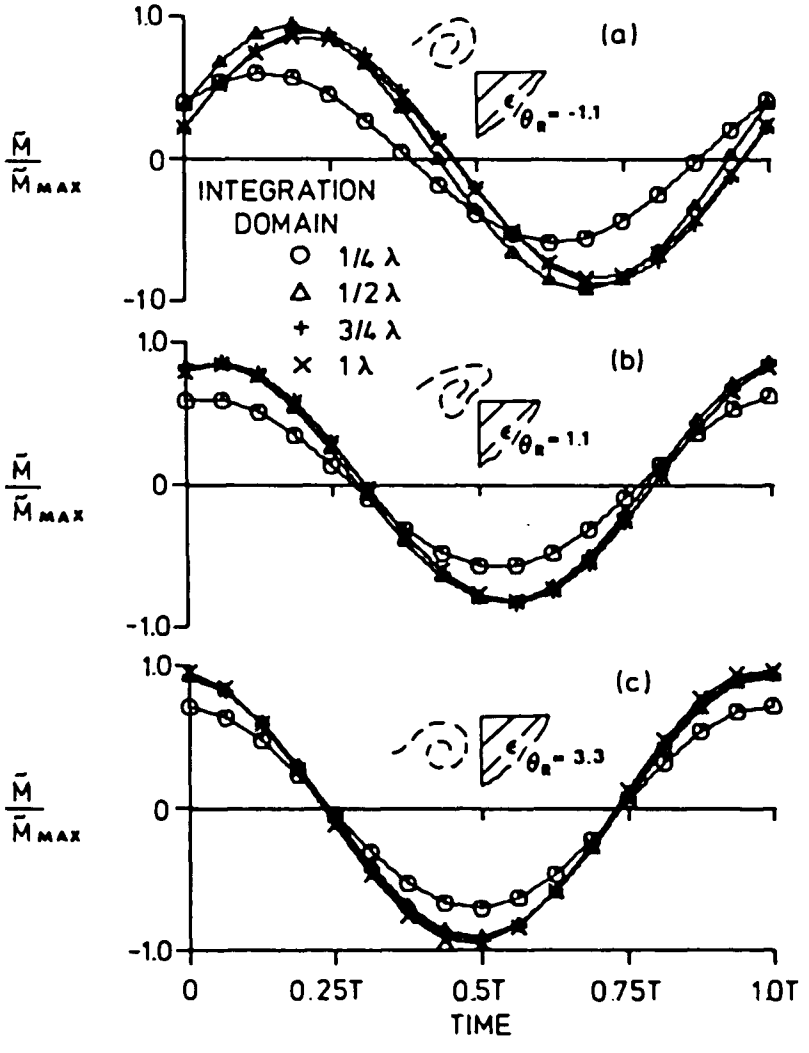

Figure 10: Fluctuating moment ($\tilde{M}$) about the intersection point ($x/\lambda = 1$ and $y/\lambda = 1$) as a function of size of integration domain for: (a) $\epsilon/\theta_R = -1.1$; (b) $\epsilon/\theta_R = 1.1$; and (c) $\epsilon/\theta_R = 3.3$. $L/\theta_R = 31$. $\tilde{M}_{max}$ has same value for all ϵ/θ_R.

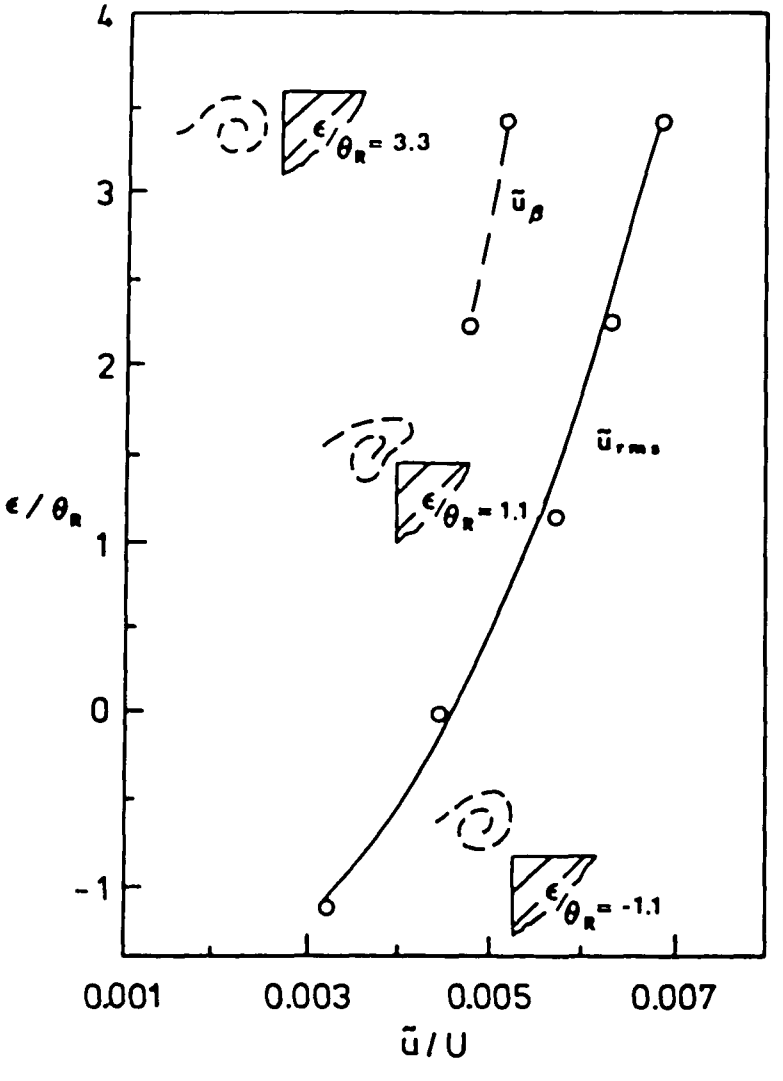

Figure 11: Root mean square of maximum longitudinal velocity fluctuation u_{rms} at separation ($x' = 0$) as a function of corner offset for $-1.1 \leq \epsilon/\theta_R \leq 3.3$.

REFERENCES

Conlisk, T. and Rockwell, D. 1981, "Modelling of Vortex-Corner Interaction Using Point Vortices", Physics of Fluids (in press).

Fuchs, H.V. 1973, Comments on "The Pressure and Velocity Fields of Convected Vortices", J. Sound and Vib. 30, 249-251.

Knisely, C. and Rockwell, D. 1981, "Self-sustained Low Frequency Components in an Impinging Shear Layer", J. Fluid Mech. (in press).

Lau, J.C., Fisher, M.J. and Fuchs, H.V. 1972, "The Intrinsic Structure of Turbulent Jets", J. Sound and Vib. 22, 379-406.

Lush, P.A. 1973, "The Pressure and Velocity Fields of Convected Vortices", J. Sound and Vib. 27, 266-270.

Michalke, A. 1965, "On Spatially Growing Disturbances in an Inviscid Shear Layer", J. Fluid Mech. 23, 521-544.

Rockwell, D. and Knisely, C. 1979 "The Organized Nature of Flow Impingement Upon a Corner", J. Fluid Mech. 93, 413-432.

Rogler, H. 1974 "A Mechanism of Vorticity Segregation", Bull. Am. Phys. Soc. Sec. II 19, 1165.

Rogler, H. 1978 "The Interaction Between Vortex-Array Representations of Free-Stream Turbulence and Semi-infinite Flat Plates", J. Fluid Mech. 87, 3, 583.

Roshko, A. 1976 "Structure of Turbulent Shear Flows: A New Look", AIAA 14, 1349-1357.

Ziada, S. and Rockwell, D. 1981 "Vortex-Leading Edge Interaction", J. Fluid Mech. (in press).

VITA

Yuk-Pui Tang was born on 3 February 1957 to Pak-Cheong Tang and Sau-King Yuen in Kowloon, Hong Kong. Yuk-Pui is the last of four children in the family. He received his high school diploma from New Method College, Kowloon, Hong Kong in May 1975.

Yuk-Pui attended Southeastern Oklahoma State University, Durant, OK for one year, then transferred to Iowa State University, Ames, IA where he received his B.S. degree in Aerospace Engineering on May 1979.

In July 1979, Yuk-Pui enrolled as a graduate student in the Department of Mechanical Engineering and Mechanics at Lehigh University, Bethlehem, PA. He also served a teaching post and research appointment during his stay. In November 1980, Yuk-Pui was privileged to present a technical paper at the thirty-third annual meeting of the American Physical Society (Fluid Dynamics Conference) at Cornell University, Ithaca, NY. Upon leaving Lehigh University, Yuk-Pui accepted employment with Air Products and Chemicals, Inc. in Allentown, PA, U.S.A.